First and Second Sound Modes of a Bose-Einstein Condensate in a Harmonic Trap

V.B. Shenoy and Tin-Lun Ho

Department of Physics, The Ohio State University, Columbus, Ohio 43210

Abstract

We have calculated the first and second sound modes of a dilute interacting Bose gas in a spherical trap for temperatures ($0.6 < T/T_c < 1.2$) and for systems with 10^4 to 10^8 particles. The second sound modes (which exist only below T_c) generally have a stronger temperature dependence than the first sound modes. The puzzling temperature variations of the sound modes near T_c recently observed at JILA in systems with 10^3 particles match surprisingly well with those of the first and second sound modes of much larger systems.

Since the discovery of Bose-Einstein condensation in atomic gases of alkali atoms [1], there has been great interest in the broken gauge symmetry (*i.e.,* the "phase") of the condensate. In the case of ^{4}He, its "phase" dynamics leads to the existence of second sound, which is essentially the out of phase pressure and temperature oscillations. In a series of sound experiments, Jin et.al at JILA [2] have observed a number of "puzzling" behaviors in the temperature dependence and the dissipation of the sound modes above $0.5T_c$. There are no explanations for these behaviors so far. Jin et.al. have speculated that the observed "$m = 0$" mode could be the "second sound". If this were true, it would be a demonstration of the broken gauge symmetry of the system. However, in the absence of a detailed calculation consistent with experiments, the identification of the second sound mode would be difficult.

To help identify the nature of the sound modes, we have solved the linearized two-fluid hydrodynamic equations of an interacting dilute Bose gas in a spherical harmonic trap. We have in mind systems that are sufficiently large so that the hydrodynamic approach is

accurate [4]. It should be noted that the recent experiments at JILA [2] were performed on small systems with a few thousand atoms. While the hydrodynamic modes of a large system may be different from the sound modes of a small one, the study of the former is important in its own right. After all, the number of atoms in the Bose condensate has increased from 10^3 to 10^6 within six months after the initial discovery [1]. It would not be surprising if Bose condensates with 10^9 atoms were produced in the near future. On the other hand, the hydrodynamic modes of large systems *are* relevant for the sound modes of small ones, as the former must evolve smoothly into the latter as the number of atoms is decreased continuously. This suggests the possibility of identifying the nature of sound modes of a small system by studying their hydrodynamic counterparts in a large one. Indeed, comparing our results (for systems with 10^4 to 10^8 atoms) with the JILA observations [2], we find that the temperature variations of the observed sound modes show up in the analogous modes of the larger systems in a spherical trap. In particular, the "mysterious" behaviors of the JILA $(m = 0)$ and $(m = 2)$ modes [2] in the range $0.5 < T/T_{co} < 0.8$ match closely with the behaviors of the second sound modes of the larger systems in same temperature range, while the frequency and temperature dependence of the observed $(m = 0)$ mode above T_c are identical to those of the first sound mode in the same temperature range. (The temperatures T_{co} and T_c are the transition temperature for the ideal Bose and the dilute interacting Bose gas respectively.) [3]

Our choice of spherical symmetry is to keep the calculations manageable. Moreover, as a first step, we shall ignore dissipation. While it is entirely feasible within our scheme to include dissipative effects, we feel that it is important (as in bulk ^{4}He) to first understand dissipationless hydrodynamics, so that one can clearly identify the dissipative effects later in a complete solution.

Linearized Hydrodynamics : We begin with the two-fluid hydrodynamic equations of Bosons with mass M in an external potential $\phi(\mathbf{r})$ [5], $M\dot{n} = -\nabla\cdot\mathbf{g}$, $\dot{g}_i = -n\nabla_i\phi - \nabla_j\Pi_{ij}$, $\dot{s} = -\nabla\cdot(s\mathbf{v}_n)$, and $\dot{\mathbf{v}}_s = -\frac{1}{M}\nabla(\mu + \phi + M\mathbf{v}_n\cdot\mathbf{v}_s)$, where n, $\mathbf{g}$, Π_{ij}, s, μ are the number density, the momentum density, the stress tensor, the entropy density, and the chemical

potential respectively. Here, $\mathbf{v}_n$ and $\mathbf{v}_s \equiv (\hbar/M)\nabla\theta$ are the normal fluid and superfluid velocities respectively, where θ is the phase of condensate. For a spherical harmonic trap with frequency ω_T, $\phi(r) = \frac{1}{2}M\omega_T^2 r^2$. In the presence of a condensate, n, $\mathbf{g}$, and Π_{ij} are of the form $n = n_s + n_n$, $\mathbf{g} = M(n_n\mathbf{v}_n + n_s\mathbf{v}_s)$, and $\Pi_{ij} = P\delta_{ij} + M(n_n v_{ni}v_{nj} + n_s v_{si}v_{sj})$, where n_s and n_n are the superfluid and normal fluid number densities, and P is the pressure. Denoting the equilibrium quantities by the subscript "$_o$", we have $\mathbf{v}_{no} = \mathbf{v}_{so} = 0$, $\nabla P_o + n_o\nabla\phi = 0$, and $\nabla(\mu_o + \phi) = 0$. Using the Gibbs-Duhem relation $d\mu = -\sigma dT + dP/n$, where $\sigma \equiv s/n$ is the entropy per particle, these equilibrium conditions imply $\nabla T_o = 0$, and hence

$$\nabla n_o = \left(\frac{\partial n}{\partial P}\right)_{T_o}\nabla P_o = -n_o\left(\frac{\partial n}{\partial P}\right)_{T_o}\nabla\phi, \qquad \nabla\sigma_o = \left(\frac{\partial \sigma_o}{\partial P}\right)_{T_o}\nabla P_o = -\frac{1}{n_o}\left(\frac{\partial n}{\partial T}\right)_{P_o}\nabla\phi, \tag{1}$$

where we have made use of the Maxwell relation $(\partial\sigma/\partial P)_T = n^{-2}(\partial n/\partial T)_P$.

Denoting the deviation of any quantity x from its equilibrium value x_o as $\delta x \equiv x - x_o$, the hydrodynamic equations can be linearized about the equilibrium solution and written as $\mathbf{I} : \delta\dot{n} = -\nabla\cdot(n_o\mathbf{v}_s + n_{no}\mathbf{w})$, $\mathbf{II} : n_o\dot{\mathbf{v}}_s + n_{no}\dot{\mathbf{w}} = -(\delta n\nabla\phi + \nabla\delta P)/M$, $\mathbf{III} : \dot{\mathbf{v}}_s = \frac{1}{M}\nabla(\sigma_o\delta T - \frac{\delta P}{n_o})$, $\mathbf{IV} : \delta\dot{s} = -\nabla\cdot(s_o\mathbf{v}_n)$, where $\mathbf{w} = \mathbf{v}_n - \mathbf{v}_s$. Using eq.(1), **I** and **II** imply that

$$M\delta\ddot{n} = \nabla\cdot\left[n_o\nabla\left(\frac{\delta P}{n_o}\right) - \delta T n_o\nabla\sigma_o\right] \equiv A. \tag{2}$$

Again using eq.(1), **II** and **III**, we have $\dot{\mathbf{w}} = -\frac{n_o\sigma_o}{Mn_{no}}\nabla\delta T$. By noting that $\dot{s} = \sigma_o\dot{n} + n_o\dot{\sigma}$, it is easy to show from **IV** that $\ddot{\sigma} = -\dot{\mathbf{v}}_n\cdot\nabla\sigma_o - \frac{\sigma_o}{n_o}\nabla\cdot(n_{so}\dot{\mathbf{w}})$, and hence

$$M\ddot{\sigma} = -(\nabla\sigma_o)^2\delta T + \frac{1}{n_o}\nabla\cdot\left(\frac{n_o n_{so}\sigma_o^2}{n_{no}}\nabla\delta T\right) + \nabla\sigma_o\cdot\nabla\left(\frac{\delta P}{n_o}\right) \equiv B. \tag{3}$$

Expressing all quantities in terms of δT and δP, Eqs.(2) and (3) form a closed set : $(\frac{\partial n}{\partial P})_T\delta\ddot{P} + (\frac{\partial n}{\partial T})_P\delta\ddot{T} = A/M$, $(\frac{\partial\sigma}{\partial P})_T\delta\ddot{P} + (\frac{\partial\sigma}{\partial T})_P\delta\ddot{T} = B/M$. The solutions of these two equations are the hydrodynamic modes of the system. To find them, we need to evaluate the thermodynamic quantities in these equations.

Thermodynamics : The thermodynamics of a trapped dilute Bose gas has been worked out within the local density approximation (LDA) by Chou, Yang and Yu (CYY) [6]. As

pointed out by CYY, LDA is valid if (a) $\epsilon \equiv \hbar\omega/k_BT << 1$, and (b) $\lambda >> a$, where $\lambda \equiv \sqrt{2\pi\hbar^2/Mk_BT}$ is the thermal wavelength and a is the s-wave scattering length. These conditions are satisfied over a very wide range of temperatures above and below T_c for large clouds. As discussed in CYY, LDA describes the physics over scales greater than $a_T \equiv \sqrt{\hbar/M\omega_T}$, and *all structures on the scale of a_T and smaller are shrunk to a point.* Since the typical width of the interface between the condensate and the normal gas is less than a_T [7], it is treated as a surface (say, at $r = r^*$) within this scheme. The density is continuous at r^* but its slope is not [6]. Because of this discontinuity, it is necessary to find the boundary conditions relating the solutions inside and outside r^*. The identification of these boundary conditions is the key to our numerical approach, and will be addressed in *Numerical Methods* below.

Further simplification can be made within the temperature range $a\lambda^2 n_o \ll 1$ (denoted as condition (c)), where all thermodynamic quantities have been worked out in the classic work of Lee and Yang [8]. Condition (c) is more restrictive than (a) above. However, it still covers a wide range of temperatures. (For a gas of ^{87}Rb with $N \sim 10^6$ in a trap with $\omega_T \sim 10^3 \mathrm{sec}^{-1}$, the condition (c) is satisfied over the range $0.6 < T/T_c < 1.2$ that we studied). The coefficients in Eqs.(2) and (3) can be calculated in a straightforward manner from ref. [6] and [8]. We shall not present the details here for length reasons. Instead, we outline the procedure and give the final expressions :

(i) To determine the density profile at temperature T_o below T_c, we first specify the chemical potential μ_o. This immediately determines the size of the condensate droplet r^* through the relation $\mu_o = \phi(r^*) + 2gn_c(T_o)$, where $n_c(T) \equiv \lambda^{-3} g_{3/2}(1)$. (ii) The region $r < r^*$ consists of both the condensate and the normal components, with $n_{no}(r) = n_c(T_o)$, and $n_{so}(r) = g^{-1}[\phi(r^*) - \phi(r)]$. The region $r > r^*$ consists of only the normal component, with $n_o(\mathbf{r})$ determined self consistently from the relation $n(\mathbf{r}) = \lambda_o^{-3} g_{3/2}(\zeta(\mathbf{r}))$, where $\ln\zeta(\mathbf{r}) = \beta[\mu_o - \phi(r) - 2gn_o(\mathbf{r})]$. The quantities N and μ_o are related though the constraint $N = 4\pi \int \mathrm{d}r r^2 [n_{so}(r) + n_{no}(r)]$. This relation combined with the condition $\mu_o = 2gn_c(T_c)$ gives T_c as a function of N.

(iii) When $a\lambda^2 n_o \ll 1$, the Hemholtz free energy is $f(n(\mathbf{r}),T) = -k_B T\lambda^{-3} g_{5/2}(1) + (g/2)[n(\mathbf{r})^2 + 2n(\mathbf{r})n_c(T) - n_c(T)^2]$ for $r < r^*$, and $f(n(\mathbf{r}),T) = -k_B T\lambda^{-3} g_{5/2}(\zeta(\mathbf{r})) + k_B T n(\mathbf{r}) \ln\zeta(\mathbf{r}) + g n(\mathbf{r})^2$ for $r > r^*$ [8]. From these two equations, it is straightforward to calculate all the thermodynamic quantities needed in Eqs.(2) and (3): for example, $P = -f + n(\partial f/\partial n)_T$ and $\sigma = s/n = -n^{-1}(\partial f/\partial T)_n$, and so forth.

Numerical Method : Since Eq.(2) and (3) are smooth inside and outside r^*, it can be solved in each of these regions in a standard way by discretizing it on a grid which is made finer as $r \to r^*$. Because some coefficients of these equations are discontinuous at r^*, (as explained before), the solution of these equations must be understood mathematically in terms of the following limiting process. Firstly, we note that the hydrodynamic equations **I** to **IV** are independent of the specific form of the free energy $f(T,n)$. We can then imagine solving these equations for a family of free energies $f(T,n;\tau)$ parametrized by a variable τ, which changes from the true free energy $f^{\rm true}$ to the LDA free energy f^{LDA} in a smooth manner as τ, say, varies from 0 to 1. Such a change, of course, amounts to gradually collapsing the actual interface into a very thin region centered at r^*. During the process of collapse, δP and δT are smooth everywhere. The most rapid changes takes place at the boundary of the interface (which we denote as $r^* \pm \Delta$), while δP and δT and their derivatives are smooth in a close neighborhood $(r^* - \epsilon, r^* + \epsilon)$ of r^* ($\epsilon << \Delta$) during the collapsing process. This implies the following (almost unique) way to implement the boundary condition : The interface is modeled by three points $r^* \pm \Delta$ and r^*, where Δ is now the grid spacing. Both δP and δT *as well as* their derivatives are continuous at r^*, while the values of δP and δT at $r^* + \Delta$ and $r^* - \Delta$ are determined by their solutions inside and outside r^*. Thus, if sharp changes ever occur in the solution, they will only occur at $r^* \pm \Delta$ and nowhere else.

As we shall see in **A** below, our numerical method reproduces a set of non-trivial modes which can also be obtained analytically. These modes exist in each angular momentum sector and are *independent of the validity of LDA*. The fact that our calculations reproduce the exact results for each ℓ shows that the boundary conditions have been implemented

correctly. [9]

Main Results : Because of spherical symmetry, δP and δT can be decomposed as $(\delta P(\mathbf{r}), \delta T(\mathbf{r})) = \sum_{\ell,n,m} (\delta P_{\ell n}(r), \delta T_{\ell n}(r)) Y_{\ell m}(\hat{\mathbf{r}})$, where ℓ is the angular momentum and n is the radial quantum number. Each (ℓ, n) mode is $2\ell+1$ fold degenerate. We have performed calculations for ^{87}Rb ($a = 58.2\mathring{A}$) for the number of trapped atoms N varying from $N = 10^4$ to 10^8. The general features of all these systems are identical. For all cases studied, we find that *the frequencies of all first and second sound are above the trap frequency* ω_T [3], which is to be expected if the system is viewed as a mechanical system with internal degrees of freedom in a harmonic potential. For concreteness, we present the results for $N = 10^6$ particles in a trap, with $\omega_T/2\pi = 200$Hz, over the range $0.6 < T/T_c < 1.2$:

(A) First sound : These modes exist both above and below T_c. They are *in phase* pressure and temperature oscillations that extend over the entire cloud, and δP has one more node than δT. The frequencies of these modes (denoted as $\omega^{(1)}_{\ell n_1}$) are shown in Fig.1 for $\ell = 0, 1, 2$ and $n_1 = 0$ to 4, where n_1 counts the number of nodes of δP in the radial direction. While $\{\omega^{(1)}_{\ell n_1}\}$ change with temperature, their variations are small compared to ω_T. The eigenfunctions of the $(\ell = 1, n_1 = 2)$ mode at $T = 0.84 T_{co}$ are shown in Fig.2a. They extend over the entire cloud – a feature common to all first sound modes above and below T_c.

The $n_1 = 0$ modes are special. They are isothermal modes of the form $\delta P(r, \hat{\mathbf{r}}) = n_o(r) r^\ell Y_{\ell m}(\hat{\mathbf{r}})$, $\delta T = 0$, with $\omega^{(1)}_{\ell,0} = \omega_T \sqrt{\ell}$. They are also "universal" in the sense that they are *independent of interaction and statistics. These results emerge from our numerical solutions* but can also be obtained analytically from Eqs.(2) and (3) . With $\delta T = 0$, using the equilibrium relations given by Eq.(1), Eqs.(2) and (3) can be shown to yield $\nabla^2(\delta P/n_o) = 0$, and $\partial_t^2(\delta P/n_o) = -\nabla\phi \cdot \nabla(\delta P/n_o)$, which has the solution given above. From the hydrdodynamic equations **I** to **IV**, it is also straightforward to show that for these isothermal modes, $\mathbf{v}_n = \mathbf{v}_s$ below T_c, and $\nabla \cdot \mathbf{v}_n = 0$ both above and below T_c.

The $(\ell = 0, n_1 = 1)$ mode is also special. Above T_c, it is a uniform temperature oscillation, $\nabla \delta T = 0$, but with $\delta T \neq 0$. This mode is "non-universal" because it depends on interactions.

The interaction effect, however, is sufficiently weak so that $\omega_{0,1}^{(1)}$ is very close to $2\omega_T$ above T_c. It is also straightforward to show that $\nabla \cdot \mathbf{v}_n$ is constant but nonzero for this mode. These results can be established analytically using LDA and also emerge as part of our numerical solutions. Below T_c, δT is no longer uniform, and $\nabla \cdot \mathbf{v}_n$ is not a constant [10]. All the other sound modes ($\ell, n_1 \neq 0$) are non-isothermal.

(B) Second Sound : These modes only exist below T_c. The frequencies of these modes for ($\ell = 0, 1, 2$) and ($n_2 = 0, 1, 2$) are shown in Fig.1. *It should be stressed that the second sound frequencies do not merge into the first sounds frequencies as* $T \to T_c$. To illustrate this clearly, we plot $\omega_{\ell,n_2=1}^{(2)}$ near T_c (for $\ell = 0$ to 2) as a function of particle number N in Fig.3. While $\omega_{\ell,n_2=1}^{(2)}$ changes with N, the first sound frequencies (not shown in Fig.3) typically vary by about 2% of ω_T in the same range of N. The eigenfunctions of the ($\ell = 1, n_2 = 2$) mode are shown in Fig.2b. An enlarged structure of the interface of this mode at r^* is shown in Fig.2c. The second sound modes have the following common features :

(1) δP and δT are "out of phase" inside the condensate and become "in phase" as they leak out into the normal region. The leakage reduces to zero as $T \to T_c$. The quantum number n_2 counts the number of nodes of δP or δT *inside* the condensate. **(2)** The wavelengths of the oscillations shrink as $r \to r^*$. This can be understood simply from LDA by recalling that the second sound velocity c_2 of a homogenous dilute Bose gas is proportional to $\sqrt{n_{so}}$. The wavelength $2\pi k^{-1}$ is then $2\pi c_2/\omega \propto \sqrt{n_{so}}$. Since $\omega \sim \omega_T$ in our case, and $n_{so}(r)$ vanishes as $r \to r^*$, the local wavelength shrinks as $r \to r^*$. **(3)** The $n_2 = 0$ modes are different from all other $n_2 \neq 0$ modes. Firstly, except very clost to T_c, all $\omega_{\ell,n_2=0}^{(2)}$ increase as T decreases, whereas all $\omega_{\ell,n_2\neq 0}^{(2)}$ have opposite behavior, (see Fig.1). Secondly, while δT and δP are out of phase for all second sound modes (i.e. $n_2 = 0$ and $n_2 \neq 0$), the sign of $\mathbf{v}_s \cdot \mathbf{v}_n$ for a particular mode depends on position. In particular, $\mathbf{v}_s \cdot \mathbf{v}_n$ of the $n_2 = 0$ modes is actually positive (i.e. in phase) almost everywhere inside the condensate instead of negative [3], whereas it can be positive or negative for the $n_2 \neq 0$ modes. (The radial components of $\mathbf{v}_s$ and $\mathbf{v}_n$ for the $n_2 \neq 0$ modes are out of phase in most regions in the condensate, so are their tangential

components. However, the in-phase and out-of-phase regions of these two components do not coincide.) This shows that unlike the second sound modes in homogenous systems, which are characterized by either out of phase (δP, δT), or out of phase ($\mathbf{v}_s$, $\mathbf{v}_n$) oscillations, *the correct characterization of the second sound modes in the trap is the out of phase δP and δT oscillations, not the out of phase $\mathbf{v}_s$ and $\mathbf{v}_n$ oscillations* [3]. **(4)** Near the center of the cloud, the ratio $\xi \equiv |n_n v_n / n_s v_s|$ is about 0.2 to 0.3 for the modes studied. This is very different from ^{4}He, where the normal current is essentially cancelled by the supercurrent, i.e. $\xi \equiv |n_n v_n / n_s v_s| \sim 1$ [3]. That ξ is between 0.2 and 0.3 can be understood in terms of LDA. From the work of Lee and Yang [11], one finds that $\xi = \frac{12}{5}(a/\lambda)(g^2_{3/2}(1)/g_{5/2}(1))$ for the homogenous dilute Bose gas, which is around 0.3 for the temperature range studied [3]. **(5)** In terms of dimensionless quantities $[\delta\tilde{P}, \delta\tilde{T}] \equiv [\delta P/(n_o(\mathbf{r})k_B T_o), \delta T/T_o]$, we find that near T_c, $\delta\tilde{T}/\delta\tilde{P} \gg 1$ for all second sound modes, whereas $\delta\tilde{P} \sim \delta\tilde{T}$ for the first sound modes.

Comparison with the JILA data: Examining the JILA data [2] on the sound modes of ^{87}Rb with $\sim 2 \times 10^3$ atoms, we find surprising consistencies with the behaviors of the larger systems that we studied : **(a)** An ($m = 0$) mode with frequency $\approx 2\omega_T$ was observed for all T above T_c [2]. The analog of this mode in a spherical trap is the ($\ell = 0, n_1 = 1$) first sound mode, which also has frequency $\approx 2\omega_T$ for all T above T_c. **(b)** Below T_c, the frequency of the ($m = 0$) mode falls from about $2\omega_T$ to $1.85\omega_T$ as T decreases from $0.9T_{co}$ to $0.5T_{co}$ [2]. The first and second sound analogs of this mode below T_c are the ($\ell = 0, n_1 = 1$) and the ($\ell = 0, n_2 = 1$) modes respectively. The observed behavior matches well with the ($\ell = 0, n_2 = 1$) second sound mode, which drops from about $1.9\omega_T$ to $1.5\omega_T$ as T decreases from $0.8T_{co}$ to $0.6T_{co}$ as seen from Fig.1. **(c)** An ($m = 2$) mode was also observed below T_c [2]. Its frequency decreases from $1.45\omega_T$ to $1.25\omega_T$ as T increases from $0.5T_{co}$ to $0.85T_{co}$. The second sound analog of this mode in spherical trap is the ($\ell = 2, n_2 = 0$) mode, which also drops from about $1.4\omega_T$ to about $1.35\omega_T$ as T increases from $0.5T_{co}$ to $0.85T_{co}$.

While we do not expect perfect agreement of our results with the JILA observations [2] because of the difference in trap symmetry and particle numbers, the qualitative and

quantitative consistencies over the temperature and angular momentum range mentioned above are striking. The above discussions suggest that the ($m = 0$) and ($m = 2$) modes observed below T_c [2] are both second sound modes. It is not clear at present why the first sound modes do not appear with great prominence below T_c. Whether it is due to the way that the modes are excited or due to the fact that density oscillations below T_c might contain a large second sound component because of the large temperature fluctuations in the second sound modes (as mentioned in Discussion **(5)** above) will be studied later. To clearly identify the nature of the sound modes, it is necessary to experimentally investigate larger number of modes so as to have more consistency checks with the hydrodynamic predictions. We hope that this work will stimulate and provide guidance for future experiments.

VBS would like to thank Allan McLeod for providing the programs on g_ν, and Vijay Shenoy and Shiwei Zhang for discussions on numerical methods. Various parts of this work were performed during TLH's regular visits to CalTech during Winter and Spring of 97. He would specially like to thank M.C. Cross for hospitality. This work is supported by NSF Grant No. DMR-9705295.

REFERENCES

[1] M.H. Anderson, *et.al.*, Science **269**, 198 (1995). C.C.Bradley, *et.al.*, Phys. Rev. Lett. **75**, 1687 (1995). K.B. Davis, *et.al.*, Phys. Rev. Lett. **75**, 3969 (1995).

[2] D.S. Jin, *et.al.*, Phys. Rev. Lett. **78**, 764 (1997).

[3] Recently, Zaremba, Griffin, and Nikuni (cond-mat/9705134) have derived the hydrodynamic equations microscopically in the Popov approximation and have found separate conservation of superfluid and normal densities. They have used a variational method to obtain the ($\ell = 1, n_2 = 0$) second sound mode. They find that the normal and supercurrents are of out phase and cancel each other, with frequencies falling below the trap frequency as $T \to T_c$. The characters of the second sound we have found are very different from theirs, (see **Main Results** and Discussions **(3)** and **(4)** below).

[4] G.M Kavoulakis, C.J. Pethick, and H. Smith, (cond-mat/9710130) have shown that 10^7 atoms are needed to reach the hydrodynamic limit near T_c for the Colorado trap.

[5] Chap.I, Sec.4 of S.J. Putterman, *Superfluid Hydrodynamics*, North Holland, 1974.

[6] T.T. Chou, C.N. Yang and L.H. Yu, Phys. Rev. A **53**, 4257 (1996).

[7] See Fig.7 of S. Giorgini, L.P. Pitaevskii, S. Stringari, cond-mat/9704014.

[8] T.D. Lee and C.N. Yang, Phys. Rev. **112**, 1419 (1958).

[9] For a given grid spacing, all eigenstates except a set denoted as $\{\omega^{(2)}_{\ell,n_2=0}\}$ below are accurate upto one part in 10^4, while those of the set are accurate upto one part in 10^3.

[10] Both $\omega^{(1)}_{\ell\neq 0,n_1=0}$ and $\omega^{(1)}_{\ell\neq 0,n_1=1}$ modes were also found by A.Griffin, W. Wu, and S. Stringari, Phys. Rev. Lett. **78**,1838 (1997) for the *ideal* Bose gas above T_c. Interaction effects and the behavior of these modes below T_c were, however, not investigated.

[11] T.D. Lee and C.N. Yang, Phys. Rev. **6**, 1406 (1959). Also see A. Griffin and E. Zaremba (cond-mat/9707058).

Figure 1: The frequencies $\omega^{(1)}_{\ell,n_1}$ and $\omega^{(2)}_{\ell,n_2}$ are represented as open and filled symbols resp. They are plotted as a function of T/T_{co}, where T_{c0} is the transition temperature of the ideal Bose gas in the trap. The dotted line at $0.917T_{co}$ indicates the critical temperature T_c of the interacting model. For the $\ell \neq 0$ modes, $r = 0$ is not counted as a node. As far as we can tell, $\omega_{\ell=0,n_2=0} = 0$.

Figure 2a: The eigenfunctions of $\omega^{(1)}_{\ell=1,n_1=2}$ (marked as A in Fig.1) : To magnify the features of the first sound, we have multiplied δP and δT by r^2 in Fig.2a.

Figure 2b: The eigenfunctions of $\omega^{(2)}_{\ell=1,n_2=2}$ (marked as B in Fig.1) : These functions are not multiplied by r^2 as those in Fig.2a because their features are sufficiently clear.

Fig.2c : The detailed structure in Fig.2b near r^*: The filled point indicates the location of r^*, and Δ is $0.005a_T$. The sharp change of slope at $r^* \pm \Delta$ is expected as our boundary condition is meant to simulate the collapsing process of LDA at r^*.

Figure 3: The N dependence of $\omega^{(2)}_{\ell,n_2=1}$ modes $(\ell, n_2 = 1)$ near T_c. The temperature is chosen so that $r^* = a_T$.

Fig.1

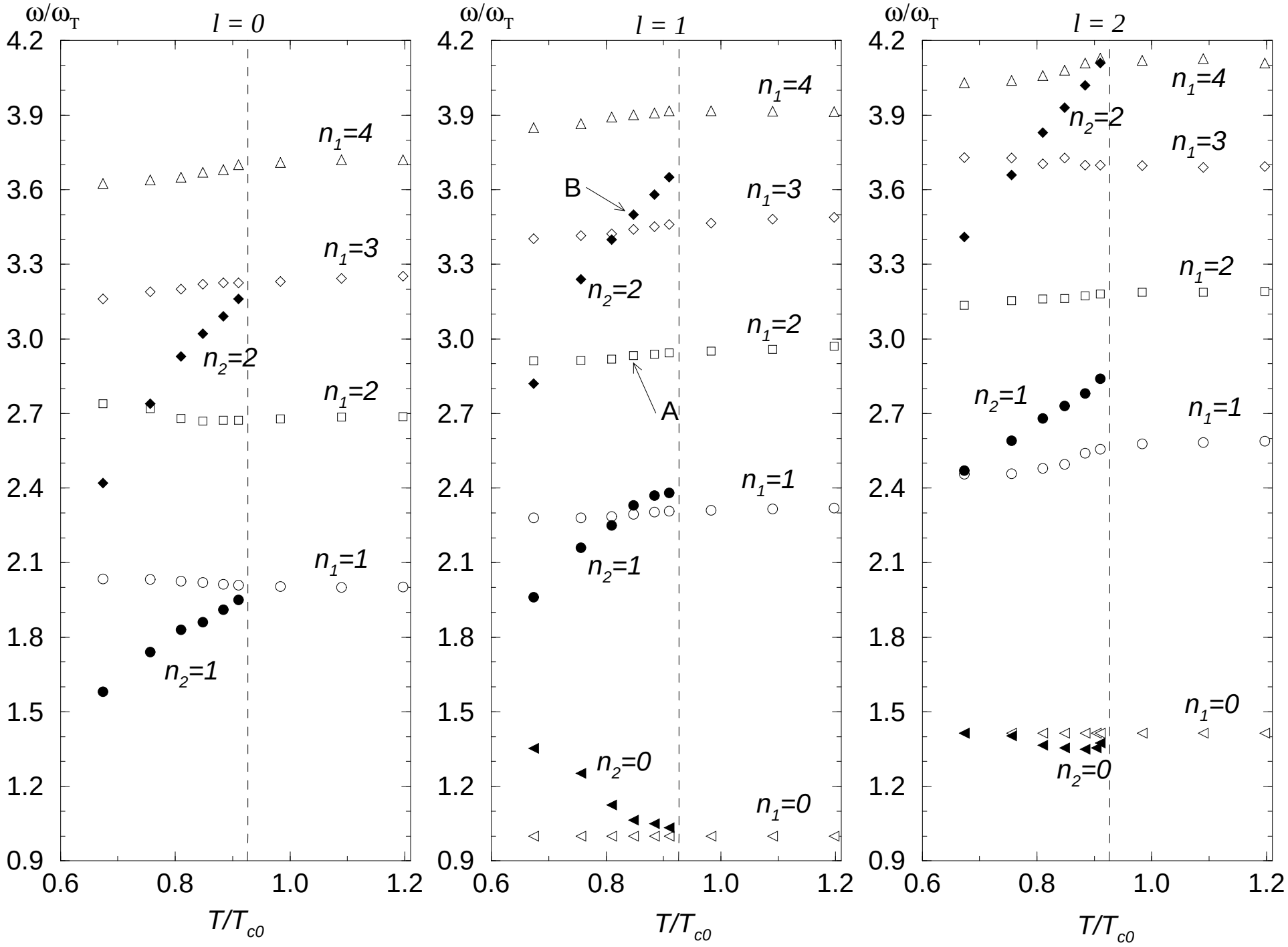
ω/ω_T
l = 0
l = 1
l = 2
n_1=4
n_1=3
n_2=2
n_1=2
n_1=1
n_2=1
n_2=0
n_1=0
n_2=2
n_1=4
n_2=2
n_1=3
n_1=2
n_2=1
n_1=1
B
A
n_1=4
n_2=2
n_1=3
n_1=2
n_2=1
n_1=1
n_1=0
n_2=0
4.2
3.9
3.6
3.3
3.0
2.7
2.4
2.1
1.8
1.5
1.2
0.9
0.6
0.8
1.0
1.2
T/T_c0

Fig.2(a)

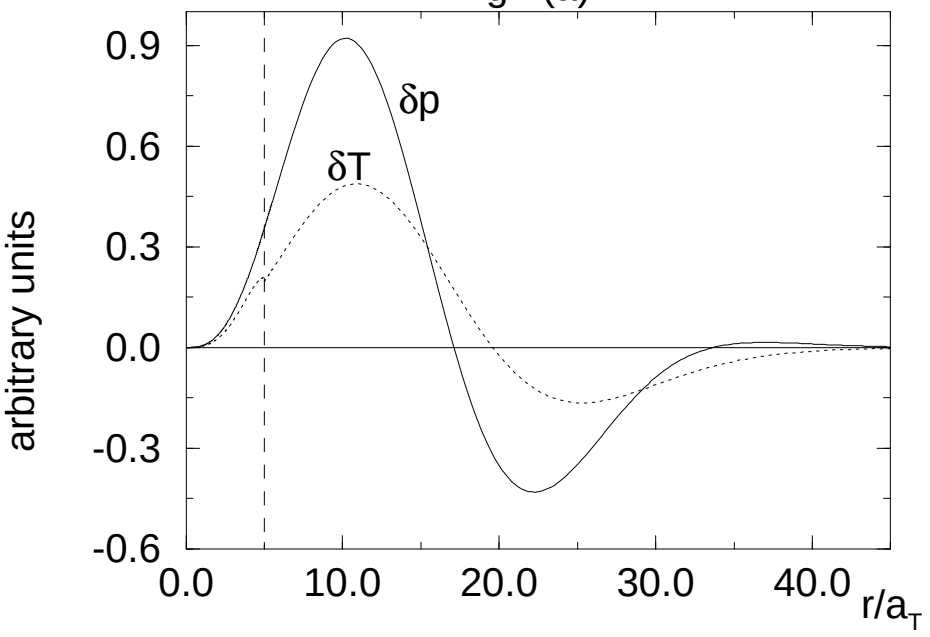

Fig.2(b)

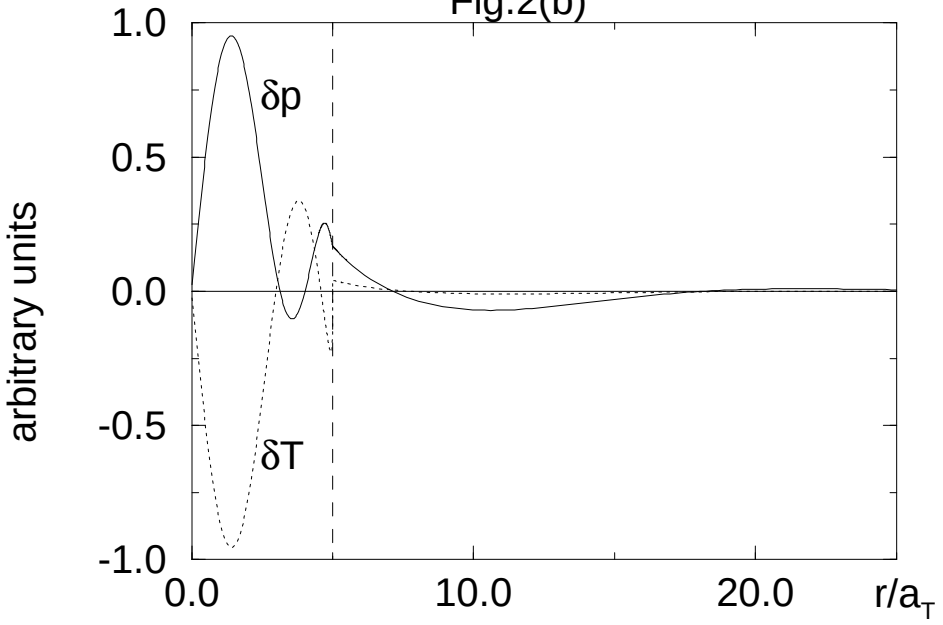

Fig.2(c)

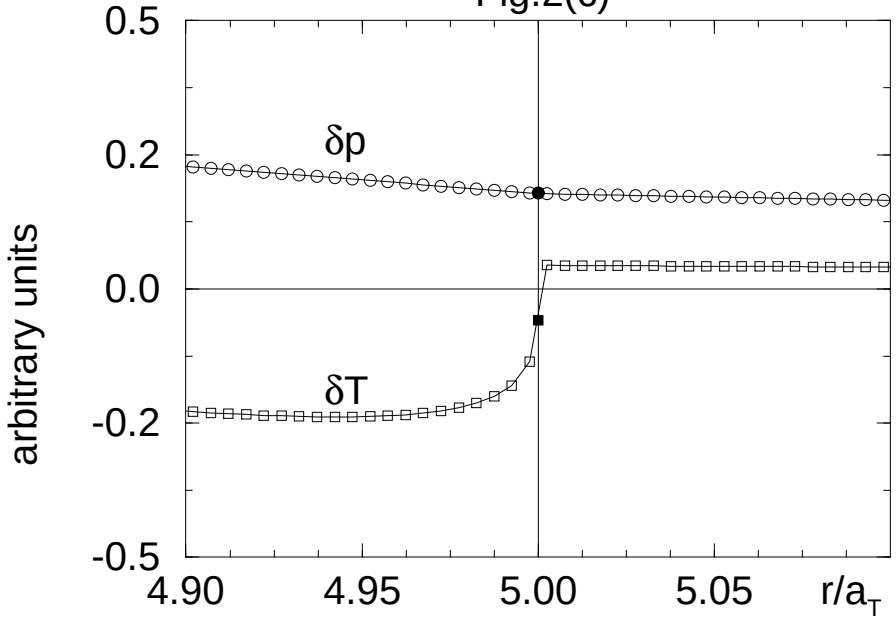

Fig.3